Metabolomic analysis of the cerebrospinal fluid reveals changes in phospholipase expression in the CNS of SIV-infected macaques

William R. Wikoff,[1] Gurudutt Pendyala,[2] Gary Siuzdak,[1] and Howard S. Fox[2]

[1]Department of Molecular Biology and Center for Mass Spectrometry and [2]Department of Molecular and Integrative Neuroscience, The Scripps Research Institute, La Jolla, California, USA.

HIV infiltrates the CNS soon after an individual has become infected with the virus, and can cause dementia and encephalitis in late-stage disease. Here, a global metabolomics approach was used to find and identify metabolites differentially regulated in the cerebrospinal fluid (CSF) of rhesus macaques with SIV-induced CNS disease, as we hypothesized that this might provide biomarkers of virus-induced CNS damage. The screening platform used a non-targeted, mass-based metabolomics approach beginning with capillary reverse phase chromatography and electrospray ionization with accurate mass determination, followed by novel, nonlinear data alignment and online database screening to identify metabolites. CSF was compared before and after viral infection. Significant changes in the metabolome specific to SIV-induced encephalitis were observed. Metabolites that were increased during infection-induced encephalitis included carnitine, acyl-carnitines, fatty acids, and phospholipid molecules. The elevation in free fatty acids and lysophospholipids correlated with increased expression of specific phospholipases in the brains of animals with encephalitis. One of these, a phospholipase A2 isoenzyme, is capable of releasing a number of the fatty acids identified. It was expressed in different areas of the brain in conjunction with glial activation, rather than linked to regions of SIV infection and inflammation, indicating widespread alterations in infected brains. The identification of specific metabolites as well as mechanisms of their increase illustrates the potential of mass-based metabolomics to address problems in CNS biochemistry and neurovirology, as well as neurodegenerative diseases.

Introduction

Early in the infection of humans with HIV, the virus infects the CNS and is detectable throughout the course of infection (1). The role of the brain in HIV-induced disease was identified initially in late-stage disease, where the clinical manifestation of HIV dementia and the neuropathological finding of HIV encephalitis were found in an appreciable number of individuals (1). In many countries, highly active antiretroviral therapy (HAART) has been successfully implemented, leading to greatly decreased mortality and prolonged course of infection. However even in the current era of treatment, the brain remains a target for damage and dysfunction: in spite of HAART lowering the overall incidence of CNS problems, the prevalence of infected individuals with CNS neurocognitive disorders has remained the same or possibly increased (2–5). This may be due in part to the fact that many HIV therapeutics do not cross the blood-brain barrier in sufficient quantity (6), as well as the now-prolonged course of infection. Though HIV does not infect neurons, it does infect myeloid-lineage cells in the brain, microglia, and macrophages, and thus the mechanism of neurological damage appears to be indirect, perhaps involving neurotoxins, inflammatory processes, viral protein–induced apoptosis, resulting in molecular and functional alterations in both neuronal and support cells in the CNS (7–9). The resulting neurological, motor, and cognitive impairments in these patients are commonly referred to as *neuroAIDS*.

Finding reliable biomarkers of HIV-induced CNS damage is important for clinical use, pharmaceutical development, and basic understanding of the mechanism of damage to the brain. The three most accessible biofluids for potential biomarker discovery are plasma, urine, and cerebrospinal fluid (CSF). CSF is the obvious choice because it is most proximal to the site of neuropathology in the brain, reflecting the biochemical milieu of the CNS.

Nonhuman primate models are an obvious alternative to studying neuroAIDS directly in humans (10). SIV infects monkeys and causes an AIDS-like disease and has many similarities to human infection, with regard to CNS involvement and neuropathological disease progression. A subset of SIV-infected rhesus monkeys develop a rapid disease course and develop a high rate of CNS disease (11). A major advantage of studying neurochemistry and other pathophysiological aspects in animal models is the greater control of the laboratory environment, minimizing extraneous variables and the number of samples. Even more important is the ability to obtain CSF samples from the same individual before and after infection.

Diverse molecular changes in the brain and CSF are associated with SIV and HIV infection and subsequent neurodegeneration. Changes in brain gene expression can be detected in the different

Nonstandard abbreviations used: CSF, cerebrospinal fluid; LC, liquid chromatography; LPC, lysophosphatidylcholine; MS, mass spectrometry; MS/MS, tandem MS; *m/z*, mass/charge ratio; PAF, platelet-activating factor; QTOF, quadrupole TOF; SIVE, SIV encephalitis.

Conflict of interest: The authors have declared that no conflict of interest exists.

Citation for this article: *J. Clin. Invest.* **118**:2661–2669 (2008). doi:10.1172/JCI34138.

Table 1
Viral load, CSF/plasma albumin ratios, and histopathology in study monkeys

Monkey	Day p.i.	Viral load (log_{10}/ml)		Albumin quotient	Histopathology
		Plasma	CSF	(CSF/plasma)	
383	133	8.5	6.9	27.9×10^{-3}	SIVE Proliferative glomerulonephritis Chronic enterocolitis
417	56	8.4	7.7	6.0×10^{-3}	SIVE Chronic colitis (mild)
418	82	8.0	7.7	24.3×10^{-3}	SIVE Proliferative glomerulonephritis SIV pneumonitis Chronic colitis (mild)
529	34	7.8	7.6	10.6×10^{-3}	SIVE Chronic colitis (mild)
404	182[A]	5.2	2.3	$< 5 \times 10^{-3}$	Chronic enterocolitis (mild)
406	182[A]	6.5	3.6	$< 5 \times 10^{-3}$	Chronic colitis (mild)
414	182[A]	5.7	2.4	$< 5 \times 10^{-3}$	Chronic colitis (mild)
423	157[A]	4.5	2.5	$< 5 \times 10^{-3}$	Meningitis (mild)

The days after inoculation (p.i.) for the terminal time point sample is given for SIVE monkeys (monkeys 383, 417, 418, and 529). [A]Time point used for metabolite analysis for animals without SIVE (monkeys 404, 406, 414, and 423), which preceded the histopathological analysis. Albumin quotients (ratios of CSF albumin concentration to plasma albumin concentration) prior to infection were normal in all animals ($<5 \times 10^{-3}$).

stages of disease (9, 12, 13). In the CSF, proinflammatory proteins such as cytokines and chemokines are increased in patients with HIV dementia (14–16). Small molecules with neurotoxic properties studied in the CSF include the tryptophan metabolites kynurenic acid and quinolinic acid (17–19), the phospholipid platelet-activating factor (PAF) (20), and the purine metabolite neopterin (21).

Metabolomics, the systems biology of small molecules, is a new approach for the untargeted identification of potential biomarkers (22). Metabolites are obvious candidates for biomarker screening because they represent the downstream effect of enzyme catalysis and other biotransformations and are smaller in number than the proteome. A particular advantage of metabolomics over targeted metabolite measurement is in hypothesis generation: the discovery of changes in molecules that were not already associated with a biological phenomenon. Although metabolomics emerged initially using NMR, mass spectrometry (MS) has evolved as a powerful technique for the comprehensive profiling of the metabolome in, for example, plasma, urine, and cells (22). The power of MS in metabolomics arises from its sensitivity, speed, and ability to interface directly with chromatography.

The application of metabolomics to viral infection or diseases of the CNS is a largely unexplored area. In the only mass-based metabolomics study of CSF in viral infection (23), 2 molecules were associated with influenza-induced encephalopathy but were not identified. Here we present one of the first mass-based metabolomics studies of CSF. Rhesus macaques were examined before and late in infection, revealing significant increases in metabolite levels during infection. This may result from pathophysiological processes such as phospholipase activation as well as breakdown of the blood-brain barrier.

Results

To determine whether the dysfunction and pathology arising in the brain following SIV infection could be detected via biochemical alterations in the CSF, a global metabolomics approach was used to examine CSF from 4 rhesus macaques before infection with SIV, late in infection, and at the time of sacrifice. These animals (Table 1) were chosen due to their symptoms of likely CNS disease (e.g., anorexia, withdrawn behavior) while alive and their documented brain pathology (i.e., SIV encephalitis [SIVE], characterized by the presence of perivascular and infiltrating macrophages, microglia/macrophage nodules, activated microglia, and multinucleated giant cells) following sacrifice. All animals progressed rapidly, requiring sacrifice due to disease between 1 and 5 months after infection. At the termination point, high levels of virus were found in both the plasma and CSF. The blood-brain barrier, assessed by comparison of albumin concentrations in both fluids, revealed leakage of albumin through the blood-brain or blood-CSF barrier in all animals.

CSF samples were extracted with methanol and applied to a capillary reverse-phase chromatography column that was interfaced to a TOF mass spectrometer; full-scan data were collected from a mass/charge ratio (m/z) of 100 to 1,000. This produced a 3-dimensional data set for each sample for time, mass, and intensity. The program XCMS (24) was used to automatically integrate chromatographic peaks, align them in the time domain, and produce a feature table consisting of m/z, retention time, and integrated intensity for each feature (Figure 1A). A "feature" is defined as an m/z–retention time pair for which a peak has been found in at least 1 group of samples and an integrated intensity has been determined.

The CSF metabolomics data set was first characterized globally. A total of 3,687 features were observed and integrated in the experiment. Significant differences were found between the uninfected and infected samples, which were analyzed as a single group (Table 2). Unequal variance t tests were calculated for each feature, with a total of 211 features found with $P \leq 0.01$. This represents 5.7% of the total number of features in the data set. When the criteria were further restricted to features with an average intensity difference of at least 1.5-fold between uninfected and infected samples, there were a total of 146 features, or 4% of the total, with $P \leq 0.01$.

Of particular interest is the extent to which the intensity data were skewed between infected and uninfected samples. When features were selected that varied by at least 50% in mean integrated intensity and that had a P value less than or equal to 0.01, then 142 of the 146, or 97% of the features increased in the infected samples relative to the uninfected ones (Table 2 and Figure 2). In other words, most of the metabolites that changed significantly increased in concentration during SIV infection and encephalitis.

A list of identified metabolites that varied significantly between uninfected and infected animals is shown in Table 3. Each metab-

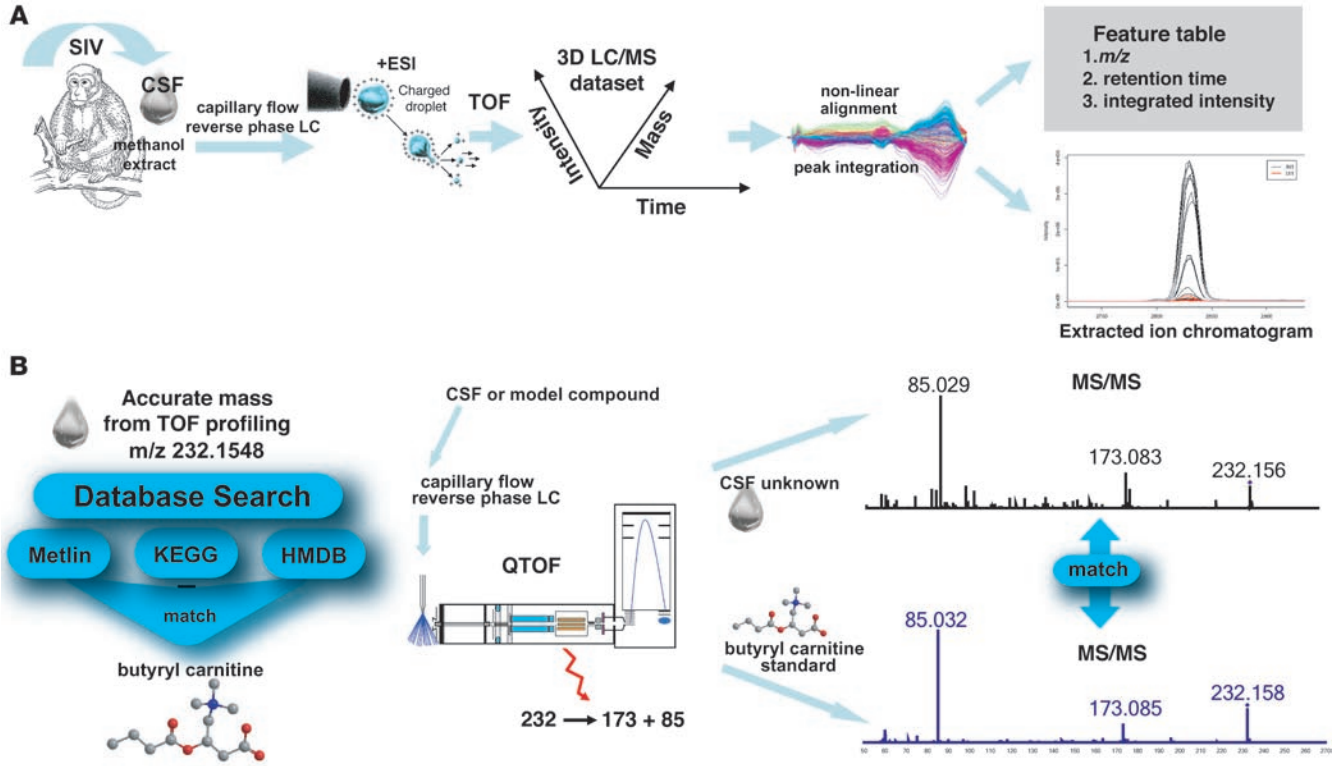

Figure 1

Metabolomics workflow. (**A**) Metabolomics profiling. Rhesus macaques were infected with SIV, and CSF was collected before and during the course of infection. Metabolites from CSF were extracted with methanol and applied to a capillary reverse-phase column at 4 μl/min. Electrospray ionization in positive mode was used, with TOF data collected from 100 to 1,000 *m/z*. Each sample produced a 3-dimensional data set. Automatic peak finding, followed by nonlinear alignment in the time domain and peak integration, was performed using the XCMS program. A feature table was produced consisting of *m/z*, retention time, and integrated intensity for each sample. An extracted ion chromatogram was automatically generated for each feature. ESI, electrospray ionization. (**B**) Identification of metabolites. Accurate mass data from metabolites of interest were obtained from the TOF data collected in the profiling experiment. Masses were searched against databases of known metabolites, such as METLIN, KEGG, and HMDB. A match provided a hypothetical identity, which was tested by obtaining fragmentation data using a QTOF instrument. The LC conditions were duplicated on the QTOF, and the CSF and model compounds were run under identical conditions, targeting the mass–retention time pair obtained from the profiling experiment. The MS/MS spectra of the unknown and model compound were compared to determine whether the 2 spectra matched. The accurate mass data, in combination with MS/MS data provided confirmation that the identity of the metabolite was correct. Numbers are *m/z* values.

olite was identified (Figure 1B) using 3 criteria: accurate mass, retention time, and tandem MS (MS/MS) data. Initially, the 146 significant features (selected as described above) were searched against the METLIN (25), HMDB (26), and KEGG (27) databases using accurate mass information; mass accuracy from the TOF was within 5 parts per million for all metabolites. Model compounds were obtained, and the retention times of these compounds were compared with the unknowns in CSF. The structures, and integrated intensities in uninfected versus infected CSF, for selected metabolites are shown in Figure 3. The identity of the metabolites was confirmed by collecting MS/MS data using a quadrupole TOF (QTOF). This approach isolates the ion with a quadrupole and then fragments it using low-energy impact with a collision gas, producing a characteristic fragmentation pattern. The MS/MS spectrum is used for identification by comparison with the fragmentation pattern of a model compound. The liquid chromatography (LC) run was repeated using the identical parameters for profiling, and fragmentation data on the target unknown metabolites were collected (Figure 1B). Molecular standards corresponding to the tentatively identified metabolites were run with the same parameters, and the MS/MS spectra were compared. The identity of 11 metabolites was confirmed using this approach (Supplemental Table 1; supplemental material available online with this article; doi:10.1172/JCI34138DS1).

Table 2

Global characterization of the metabolomics data

Parameter	No. of features[A]
Total observations	3,687
Observations with $P \leq 0.01$	211
Observations with $P \leq 0.01$ and fold change ≥1.5	146
Observations with $P \leq 0.01$ and fold change ≥1.5, number (%) up in infected	142 (97.3%)
Observations with $P \leq 0.01$ and fold change ≥1.5, number (%) down in infected	4 (2.7%)

[A]Defined as an *m/z*–retention time pair for which a peak has been found in at least 1 group of samples in the data set and integrated. *P* values compare uninfected and infected integrated intensities.

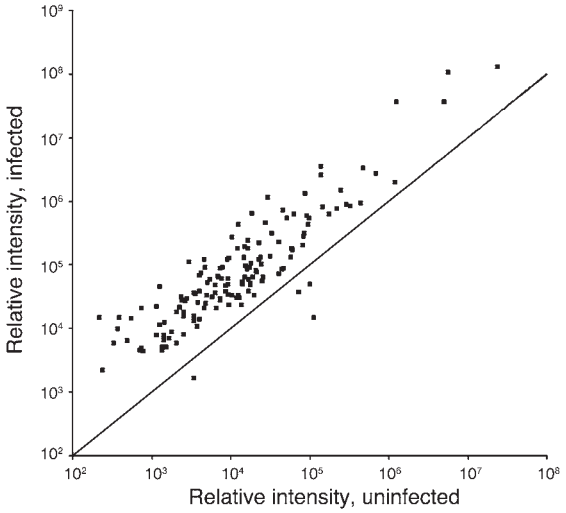

Figure 2
Scatter plot comparing integrated intensities of the 146 significant molecular features for uninfected versus infected samples. Ions were selected with a fold difference ≥1.5 and $P \leq 0.01$. The diagonal line represents the equation $y = x$, so that points above the line represent the 142 metabolites that increase in concentration in infected samples, which is 97% of the total.

Four different categories of molecules were elevated in infection: carnitine and acyl-carnitines, fatty acids, and phospholipids. The level of carnitine increased in infection by an average of 9.1-fold. In addition, 3 acyl-carnitines, isovaleryl, butyryl, and octanoyl carnitine increased by 3.7- to 10.4-fold. An increase in the concentration of 5 saturated and unsaturated fatty acids in CSF was found in infection as well, with increases ranging from 3.0- to 35.5-fold (in the case of palmitic acid). Three of these 6 are the constituent fatty acids of lysophosphatidylcholine (LPC) phospholipids, which were increased by 26.3- to 73.9-fold.

The finding of metabolic changes in SIV-infected animals that had progressed to neuroAIDS raises the question of the precise etiology of the changes: whether they are the result of SIV infection or are specifically related to neurological involvement and encephalitis. To determine whether the changes in the metabolome were indeed specific to the neurological involvement and encephalitis, a second set of animals was examined. CSF was collected before infection and approximately 6 months after infection from animals that did not progress to encephalitis (Table 1). A targeted LC/MS approach (multiple reaction monitoring [MRM]) was used to profile the specific metabolites that changed in encephalitis (Table 3, *P* values and fold changes shown in parentheses). There was no significant change in metabolite levels in animals that lacked neurological symptoms (and did not have encephalitis at sacrifice) 6 months after infection. This indicates that the metabolic changes observed in late-stage infection are specifically related to SIV-induced encephalitis.

This increase in certain molecules in the CSF, some of which are known to be present in higher concentrations in plasma than in CSF (28–31), may result from a selective compromise of the blood-brain or blood-CSF barrier, and we indeed found albumin to be elevated in the CSF of encephalitic animals. However the identification of numerous free fatty acids and lysophospholipids may also reflect increased phospholipases in the SIV-infected brain. Examination of global gene expression changes in hippocampal RNA (assessing uninfected animals and those with SIVE using a rhesus monkey sequence-specific gene array; H.S. Fox, unpublished observations) revealed that the expression of 2 phospholipases was significantly changed (following normalization by robust multi-array analysis; ≥2-fold difference between the groups; $P < 0.01$), and both were increased in animals with SIVE: phospholipase A1 member A (PLA1A) and phospholipase A2 group IVC (PLA2G4C). To determine whether these were indeed upregulated in the 4 animals analyzed here, we performed quantitative real-time PCR analysis on hippocampal RNA from these monkeys as well as 9 uninfected monkeys, revealing a significant 9.3-fold upregulation of PLA1A and 6.4-fold upregulation of PLA2G4C ($P = 0.049$ and $P = 0.019$, respectively, unequal variance *t* test) (Figure 4).

Table 3
Selected metabolites

Name	Molecular formula	*m/z* observed	*m/z* calculated	Relative error (ppm)	Retention time (min)	*P* value	Fold change
Carnitine	$C_7H_{15}NO_3$	162.1124	162.1125	–0.62	2.9	0.010 (0.52)	9.1 (1.1)
Isovaleryl carnitine	$C_{12}H_{23}NO_4$	246.1694	246.1699	–2.44	12.5	0.007 (0.35)	9.9 (1.2)
Octanoyl carnitine	$C_{15}H_{29}NO_4$	288.2173	288.2169	1.04	23.9	0.005 (0.29)	3.7 (1.3)
Butyryl or isobutyryl carnitine	$C_{11}H_{21}NO_4$	232.1548	232.1544	1.72	7.1	<0.001 (0.36)	10.4 (1.8)
Palmitic acid (C16:0)	$C_{16}H_{32}O_2$	257.2478	257.2475	1.17	47.2	0.011 (0.58)	35.5 (1.2)
Oleic acid (C18:1)	$C_{18}H_{34}O_2$	283.2634	283.2632	0.71	39.5	0.029 (0.97)	2.5 (1.0)
Linoleic acid (C18:2)	$C_{18}H_{32}O_2$	281.2472	281.2475	–1.07	40.7	0.004 (nd)	3.2 (nd)
Stearic acid (C18:0)	$C_{18}H_{36}O_2$	285.2793	285.2788	1.75	50.9	0.005 (0.37)	14.4 (0.7)
Myristic acid (C14:0)	$C_{14}H_{28}O_2$	229.2164	229.2162	0.87	43.0	0.009 (0.20)	5.5 (1.2)
LPC (16:0)	$C_{24}H_{50}NO_7P$	496.3373	496.3398	–5.04	38.6	0.039 (0.59)	26.3 (1.2)
LPC (18:2)	$C_{26}H_{52}NO_7P$	522.3542	522.3554	–2.30	39.5	0.042 (0.61)	27.5 (1.2)
LPC (18:0)	$C_{26}H_{54}NO_7P$	524.3720	524.3711	1.72	43.5	0.038 (0.44)	73.9 (1.4)

Twelve metabolites were identified from the features that changed following SIV infection, based on mass accuracy and retention time. The observed and calculated *m/z* are given, with the differences shown in parts per million (ppm). The fold change reflects the average increase in samples taken after infection. *P* values (obtained using *t* test) and fold changes for animals that did not progress to encephalitis are shown in parentheses. nd, not determined.

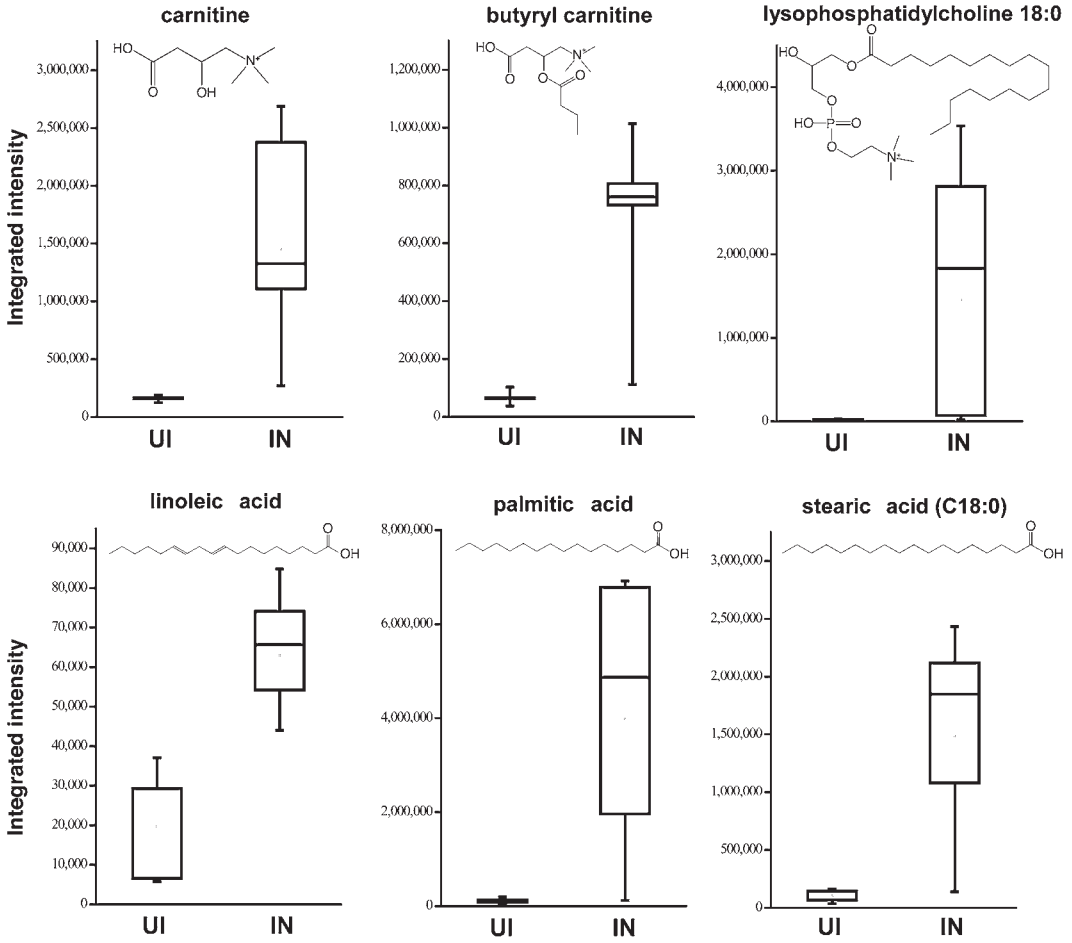

Figure 3
Box-and-whisker plots showing integrated intensities for selected ions in uninfected (UI) versus infected (IN) CSF, and proposed structures of the metabolites. Bottom and top of the boxes indicate 25th and 75th percentiles, and whiskers indicate 5th and 95th percentiles.

In order to further examine the expression of these phospholipases in the brains of monkeys with SIVE, we cloned their rhesus cDNA sequences and used them as probes for in situ hybridization experiments. Although no signal was detected for PLA1A, perhaps due to sensitivity issues, PLA2G4C was strongly expressed in the brains of animals with SIVE (antisense probe, Figure 5, A and D–F; sense negative control, Figure 5B) but not in the brains of uninfected animals (antisense probe, Figure 5C). Interestingly, although expression was detected in the characteristic macrophage/microglia nodules and perivascular infiltrates (Figure 5, D and E), expression was not strongly localized to these inflammatory lesions and could be found in neuronal-rich areas such as the hippocampus (Figure 5A), in subcortical white matter (data not shown), and along the ventricular lining and choroid plexus (Figure 5F). Glial activation was present in areas where PLA2G4C expression occurred (microglia stained for CD163, Figure 5G; astrocytes stained for GFAP, Figure 5H) but was not linked to regions of viral infection; for example, only rare SIV-positive cells (stained for SIV p27 Gag) could be found in the vicinity of the hippocampal section shown in Figure 5I, compared with abundant SIV-positive cells in the macrophage/microglia nodules (Figure 5J).

Discussion

We have found an increase in concentration of large numbers of metabolites in the CSF of animals with SIV-induced CNS disease, which to our knowledge have not been previously observed in SIV or HIV infection. The identified metabolites do not share any obvious structural or chemical characteristics that would suggest a single, simple biochemical mechanism for their increase. For example, carnitine and acyl-carnitines are polar, small, and cationic in solution, whereas fatty acids are negatively charged and somewhat hydrophobic, and LPCs are larger and amphipathic. However, there is a possible biochemical relationship between these molecules via the fatty acid oxidation pathway, involving fatty acids, carnitine, and acyl-carnitines, as the conjugation of fatty acids to carnitine is required for transport of long-chain fatty acids across the mitochondrial membranes.

Several of these metabolites have been linked to other CNS disorders. Carnitine was found in one study to increase 2- to 3-fold in CSF in children with meningitis, neurological disorders, and seizures, conditions associated with neuropathology (32). However, in studies of Alzheimer (33) and Parkinson (34) diseases, neither free nor acyl-carnitine levels significantly correlate with disease. Free fatty acids were shown to increase in patients with traumatic brain injury (35), stroke (36), and subarachnoid hemorrhage (37), yet a decrease in fatty acid concentrations was demonstrated in multiple sclerosis (38) and Alzheimer disease (39).

Changes in specific metabolite levels in CSF have, however, previously been associated with SIV or HIV infection. For example the concentration of the neurotoxic metabolite quinolinic acid, part of the kynurenine pathway, was shown to increase in CSF during infection with HIV and SIV (19, 40) and other neuroinflammatory

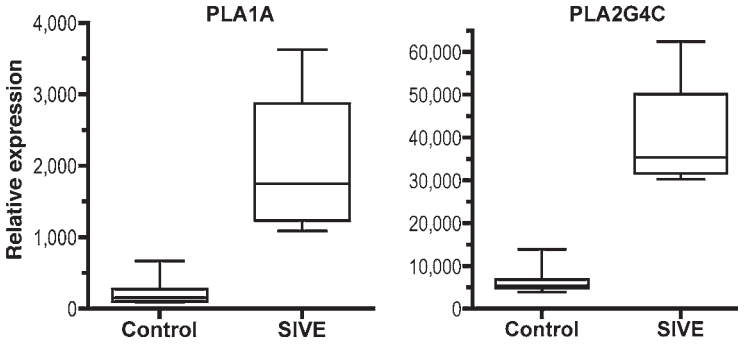

Figure 4
Box-and-whisker plots showing relative values for gene expression for the indicated phospholipase genes in the hippocampus of 9 uninfected rhesus monkeys as controls, compared with the 4 SIVE animals used in this study. Bottom and top of the boxes indicate 25th and 75th percentiles, and whiskers indicate 5th and 95th percentiles.

diseases (41). The nitric oxide metabolites nitrate and nitrite are increased in a similar fashion (42–44).

The most obvious explanation for the significant increase in metabolites between uninfected and infected animals is a compromise of blood-brain barrier integrity and an increase in its permeability to certain small-molecule compounds. A compromise of the blood-brain barrier does occur in both SIV (45, 46) and HIV infection (47, 48), and indeed, we found an increase in albumin in the CSF. It will be interesting to examine the CSF metabolome in other CNS conditions in which the blood-brain barrier is or may be compromised, such as brain trauma (49), Alzheimer and Parkinson diseases (50), multiple sclerosis (51), and other infections that result in encephalitis and/or meningitis.

However, considering fatty acid entry, production, and metabolism in the CNS, the interpretation is likely more complex (31, 52). Both diffusion and carrier-mediated transport systems enable blood-born free and esterified fatty acids to enter the brain, and the brain can also synthesize fatty acids. Free fatty acids found in the CSF can result from entry of blood-borne fatty acids across the choroid plexus. The CSF also serves as a sink for fatty acids, which are a product of normal brain metabolism, as well as the increase found in conditions such as those resulting from genetic enzyme deficiency or in a number of inflammatory CNS pathologies. The latter are likely the result of increased brain phospholipase activity, resulting in the production of free fatty acids and lysophospholipids (53).

Indeed, in the SIVE brain we have found that 2 phospholipases are increased. PLA1A is a secreted enzyme that hydrolyzes phosphatidylserine and 1-acyl-2-lysophosphatidylserine to produce 2-acyl-1-lysophosphatidylserine, glycerophosphoserines, and free fatty acids (54). PLA2G4C is a membrane-associated enzyme that sequentially hydrolyzes fatty acid from the *sn*-2 and *sn*-1 positions of phosphatidylcholines, releasing lysophosphatidylcholine in addition to saturated and unsaturated fatty acids. In contrast to the well-characterized PLA2A, PLA2G4C does not show specificity for arachidonic acid and can release large amounts of oleic and palmitic acids (55), both of which we found to be increased in the CSF in animals with SIVE.

The expression of PLA2G4C was further investigated by in situ hybridization experiments. Interestingly, cells expressing relatively high levels of this molecule could be found throughout the brain and were not strictly linked to areas with inflammation and/or proximity to SIV-infected cells. While many untoward effects of products of virus-infected macrophage/microglia have been identified, the induction of PLA2G4C, and subsequent production of metabolites, appears unrelated spatially to these pathological lesions, indicating more widespread alterations in infected brains.

Neither PLA1A nor PLA2G4C require posttranslational modifications, such as phosphorylation, for enzymatic activity. Therefore, the free fatty acids and lysophospholipids found here can reflect a pathological increase in phospholipases, which have ample sub-

Figure 5
Photomicrographs of in situ hybridization and immunohistochemical analyses. (**A**–**F**) In situ hybridization experiments. In brains with SIVE, hybridization with an antisense probe (**A**) to PLA2G4C revealed abundant positive cells (black grains indicate a positive signal), indicating active transcription of this phospholipase, whereas hybridization to the sense probe (negative control) (**B**) did not. Hybridization of the antisense probe to brains from uninfected monkeys (**C**) did not reveal positive cells. The PLA2G4C antisense probe also reacted with cells in macrophage/microglia nodules (**D**) and perivascular inflammatory infiltrates (**E**). In addition to the brain parenchyma, positive cells were found along the ventricular lining and in the choroid plexus (**F**). (**G**–**J**) Immunohistochemical staining experiments (reddish-brown staining indicates a positive signal). In brains with SIVE, reactive/activated microglia (CD163) (**G**) and astrocytes (GFAP) (**H**) were found in areas of PLA2G4C expression. However, only rare cells expressing SIV were found (SIV p27 Gag) (**H**), although in macrophage/microglia nodules there was plentiful SIV expression (SIV p27 Gag) (**I**). Original magnification, ×25 (**A**–**H**) and ×40 (**I** and **J**).

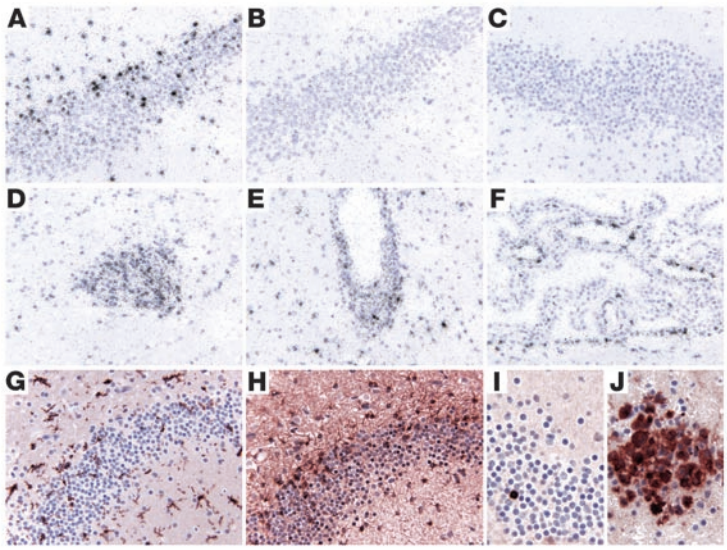

strates in the lipid-rich environment of the brain. Additional evidence for alterations in phospholipid metabolism, focusing on sphingomyelins, has been found in studies on HIV-infected brain and CSF samples as well as in in vitro systems (56).

Furthermore, many of these molecules themselves can induce receptor signaling, thus further altering CNS function. Free fatty acids can signal through GPCR40 (57) as well as through the nuclear receptor PPARα (58). LPC itself, and its metabolic product lysophosphatidic acid, are ligands for a number of GPCRs (59); additionally LPC is a precursor for PAF, which has its own GPCR and can lead to neuronal damage (60). LPC also increases microglial release of IL-1β (61), a key cytokine in neurodegenerative and neuroinflammatory disorders including HIV dementia.

In summary, we have successfully applied a global metabolomics approach to assess the CSF in a neurodegenerative disease of primates. In SIV-induced CNS disease in monkeys, we found significant changes in the CSF metabolome and identified specific upregulated metabolites that not only can have neuropathogenic effects, but also indicate mechanisms of disease. Increased expression of specific phospholipases, which are capable of producing a subset of the identified metabolites, was found in the brains. Similar studies in other neurodegenerative as well as neuropsychiatric disorders have the potential to address the physiological disruptions underlying CNS diseases.

Methods

Monkeys and SIV. Rhesus monkeys were intravenously inoculated with a cell-free stock of SIV derived from SIVmac251 (62, 63). CSF samples were taken from the cisterna magna by percutaneous puncture while animals were under ketamine anesthesia. Blood was obtained from the femoral vein and anticoagulated in EDTA for plasma isolation. Cells were removed from CSF by centrifugation and the supernatant stored at –80°C. The 4 animals utilized for the initial metabolomic profiling all developed rapidly progressing simian AIDS, necessitating sacrifice within 6 months following viral inoculation. Monkeys were sacrificed due to predetermined criteria including progressive weight loss, marked hematological abnormalities, persistent anorexia, diarrhea not responsive to treatment, and the presence of neurological or behavioral signs. All had SIVE upon histopathological analysis. The 4 animals utilized for assessing specificity of the metabolic changes to SIVE were sacrificed per experimental protocol between 6.5 and 22 months following viral inoculation and had no neuropathology. Complete histopathological examination was performed on tissues from all monkeys. These studies were conducted following approval of The Scripps Research Institute's IACUC and were in accordance with NIH guidelines.

CSF was collected from all animals before infection (uninfected sample) and at regular intervals following infection. From the animals that developed simian AIDS, CSF was analyzed from the sample taken at sacrifice at the terminal stage of disease. In 3 of the monkeys (monkeys 383, 417, and 418), an additional post-infection sample, taken 5–25 days before sacrifice, was also analyzed. From the animals that did not develop SIVE CSF, the CSF sample from 5–6 months following viral inoculation was used, in addition to an uninfected sample, for analysis. Viral load was determined in the CSF and plasma using the bDNA assay by Siemens Reference Lab. Albumin concentrations in the CSF and plasma were determined using a radial immunodiffusion test kit (The Binding Site). The albumin quotient (CSF albumin concentration divided by serum albumin concentration) was calculated as a measure for blood-brain barrier integrity; our previous studies indicated that uninfected animals have an albumin quotient of less than 5×10^{-3} (64).

CSF metabolomics. Metabolites were extracted from CSF with methanol. Four volumes of cold methanol were added to 100 μl of CSF, vortexed, and incubated at –20°C for 1 hour. Samples were centrifuged 10 min at 14,000 *g*, the supernatant was collected, and the centrifugation was repeated. The supernatant was dried in a SpeedVac and resuspended in 50 μl (2× concentrated relative to original volume) 95:5 water/acetonitrile and clarified for 5 min at 14,000 *g*.

Extracted CSF (8 μl) maintained at 4°C in an autosampler was applied to a capillary reverse-phase column (Zorbax C18; Agilent) with dimensions of 300 μm internal diameter × 150 mm length. The flow rate was 4 μl/min with solvent A composed of water containing 0.1% formic acid, and solvent B composed of acetonitrile containing 0.1% formic acid. The gradient consisted of 5% solvent B for 5 min, followed by a gradient to 95% solvent B over 45 min, held at 95% solvent B for 5 min, and re-equilibrated at 5% solvent B for 10 min.

To reduce systematic error associated with instrument drift, samples were run in an order that alternated between uninfected and infected. Each sample was run in duplicate, and after data integration, duplicate runs were averaged. Data were collected in positive electrospray mode on a TOF (Agilent) operated in full-scan mode at 100 to 1,000 *m/z*. The capillary voltage was 3,500 V with a scan rate of 0.5 scans/s; nebulizer flow was 12 l/min. Data in instrument-specific format were converted to CDF format files. The program XCMS (24) was used for nonlinear alignment of the data in the time domain and automatic integration and extraction of the peak intensities. Accurate masses of features representing significant differences were searched against the METLIN (25), HMDB (26), and KEGG databases (27).

Metabolite identification. The following compounds for confirmation of metabolite ID were obtained from Sigma-Aldrich (CAS no.): L-carnitine (6645-46-1), palmitic acid (57-10-3), oleic acid (112-80-1), linoleic acid (60-33-3), stearic acid (57-11-4), myristic acid (544-63-8), lysophosphocholine (16:0) (17364-16-8), lysophosphocholine (18:2) (19420-56-5), and lysophosphocholine (18:0) (19420-57-6). Hexanoyl carnitine (6418-78-6) and butyryl carnitine (25576-40-3) were a generous gift from Jon Gangoiti, UCSD.

For confirmation of metabolite identification, samples of infected CSF or model compounds to be tested were run under chromatographic conditions similar to those of the profiling experiment, except that the flow rate was 6 μl/min. Data were collected using an Agilent 6510 QTOF, with gas temp of 350°C, drying gas flow of 4 l/min, nebulizer pressure of 15 psi, capillary voltage of 3,500 V, fragmentor voltage of 120 V, and skimmer voltage 60 V. MS spectra were collected at 2 spectra/s, and MS/MS spectra were collected at 0.5 spectra/s, with a medium isolation window (~4 *m/z*) and a fixed collision energy of 15 V.

Multiple reaction monitoring of identified metabolites. To determine whether the changes in the metabolome were specific to neurological involvement and encephalitis, a second set of animals was examined. CSF was collected at approximately 2 weeks prior to infection and 5–6 months following infection from animals that did not progress to encephalitis. CSF was extracted using methods identical to those used for the first group. Metabolites identified were profiled using LC/MS with a triple quadrupole (Agilent 6410) targeting the multiple reaction monitoring (MRM) transitions (developed from authentic standards) for carnitine (*m/z* 162→103.0, 60.1; collision energy, 15), acyl-carnitines (precursor→85, 60; collision energy, 15), and lysophosphatidyl cholines (precursor→184, 104; collision energy, 20), where the MRM transition is indicated by an arrow (precursor→product). Fatty acids were targeted using single-ion monitoring. CSF extract (5 μl) was injected, with a 20-min gradient from 5% to 95 % solvent B, using the same column and mobile phases that were used for profiling. Peaks were automatically integrated using instrument software.

Quantitative real-time PCR. RNA was isolated from hippocampal samples taken following necropsy using TRIzol reagent (Invitrogen) and then further purified utilizing the RNeasy mini kit (Qiagen). RNA was incubated

with random primers and SuperScript II reverse transcriptase (Invitrogen), followed by heat inactivation and treatment with RNaseH (New England BioLabs). Specific RNA transcripts were quantified through the use of real-time PCR using dual-labeled (FAM-TAMRA) hydrolysis probes. Reactions were optimized and validated by dilutional analysis. Primer and probe sequences are available in Supplemental Table 2. Primers and probes were obtained from Eurogentec. Quantitative real-time PCR reactions were performed using Platinum qPCR UDG Supermix (Invitrogen) in an MX3000 machine (Stratagene). Reactions were performed in duplicate. To compute the relative amounts of *PLA1A* and *PLA2G4C* mRNA in the samples, the average Ct of the primary signals for the TATA-box binding protein, glyceraldehyde-3-phosphate dehydrogenase, and 18S ribosomal RNA (used as controls) was subtracted from that of PLA1A or PLA2G4C to give the change in Ct (dCt), and relative values were calculated as 2^{dCt}.

Histopathological analysis: in situ hybridization and immunohistochemistry. Brain tissue was fixed for 48 hours in formalin and then embedded in paraffin. Sections 6 μm long were cut from the paraffin blocks, mounted on glass slides, and either subjected to hematoxylin and eosin staining (Sigma-Aldrich), in situ hybridization analysis, or immunohistochemical staining. In situ hybridization analysis was performed as previously described (65) using ^{35}S-labeled single-strand RNA probes consisting of fragments of the rhesus monkey PLA1A or PLA2G4C, obtained by RT-PCR amplification using oligonucleotides derived from the homologous GenBank sequences, cloned into a vector with opposable RNA bacteriophage promoters, and sequence verified. In addition to the antisense probe hybridization, controls included sense probe hybridization. The slides were exposed to emulsion for 11 days before development. Immunohistochemical staining followed a basic indirect protocol, using an antigen retrieval method as previously described (65). Primary antibodies were mouse monoclonal anti-CD163 (Novocastra) and anti-SIV p27 Gag (produced in our laboratory from the FA2 hybridoma provided by the NIH AIDS Research and Reference Reagent Program) and rabbit polyclonal anti-GFAP (Zymed Laboratories).

Image capture was performed with a Spot RT Color CCD camera with Spot RT software version 3.4.2 for MacOS (Spot Diagnostic Instruments) using a Leica Diaplan microscope (Leica Inc.). Figures were assembled with Adobe Photoshop, version 6.0 for MacOS (Adobe Systems Inc.).

Statistics. All *t* tests were 2-tailed Welch's *t* tests with unequal variance and were calculated using Microsoft Excel. Box-and-whisker plots were calculated using Origin 6.1 (OriginLab).

Acknowledgments

We thank Debbie Watry, Claudia Flynn, and Michelle Zandonatti for technical assistance. The SIVmac p27 hybridoma FA2 from Suganto Sujipto and Preston Marx was obtained through the AIDS Research and Reference Reagent Program, Division of AIDS, NIAID, NIH. This is manuscript no. 19184 from The Scripps Research Institute. This work was supported by NIH grants MH062261 and MH073490.

Received for publication October 3, 2007, and accepted in revised form April 16, 2008.

Address correspondence to: Howard S. Fox, The Scripps Research Institute, 10550 North Torrey Pines Road, SP30-2030, La Jolla, California 92037, USA. Phone: (858) 784-7171; Fax: (858) 784-7296; E-mail: hsfox@scripps.edu or hfox@unmc.edu. Or to: Gary Siuzdak, The Scripps Research Institute, 10550 North Torrey Pines Road, SR-15, La Jolla, California 92037, USA. Phone: (858) 784-9415; Fax: (858) 784-9496; E-mail: siuzdak@scripps.edu.

1. Ellis, R., Langford, D., and Masliah, E. 2007. HIV and antiretroviral therapy in the brain: neuronal injury and repair. *Nat. Rev. Neurosci.* **8**:33–44.
2. Sacktor, N., et al. 2002. HIV-associated cognitive impairment before and after the advent of combination therapy. *J. Neurovirol.* **8**:136–142.
3. Dore, G.J., McDonald, A., Li, Y., Kaldor, J.M., and Brew, B.J. 2003. Marked improvement in survival following AIDS dementia complex in the era of highly active antiretroviral therapy. *AIDS.* **17**:1539–1545.
4. Cysique, L.A., Maruff, P., and Brew, B.J. 2004. Prevalence and pattern of neuropsychological impairment in human immunodeficiency virus-infected/acquired immunodeficiency syndrome (HIV/AIDS) patients across pre- and post-highly active antiretroviral therapy eras: a combined study of two cohorts. *J. Neurovirol.* **10**:350–357.
5. Tozzi, V., et al. 2005. Prevalence and risk factors for human immunodeficiency virus-associated neurocognitive impairment, 1996 to 2002: results from an urban observational cohort. *J. Neurovirol.* **11**:265–273.
6. Letendre, S.L., et al. 2004. Enhancing antiretroviral therapy for human immunodeficiency virus cognitive disorders. *Ann. Neurol.* **56**:416–423.
7. Gendelman, H.E., Lipton, S.A., Tardieu, M., Bukrinsky, M.I., and Nottet, H.S. 1994. The neuropathogenesis of HIV-1 infection. *J. Leukoc. Biol.* **56**:389–398.
8. Kaul, M., Garden, G.A., and Lipton, S.A. 2001. Pathways to neuronal injury and apoptosis in HIV-associated dementia. *Nature.* **410**:988–994.
9. Roberts, E.S., et al. 2003. Induction of pathogenic sets of genes in macrophages and neurons in NeuroAIDS. *Am. J. Pathol.* **162**:2041–2057.
10. Burudi, E.M., and Fox, H.S. 2001. Simian immunodeficiency virus model of HIV-induced central nervous system dysfunction. *Adv. Virus Res.* **56**:435–468.
11. Westmoreland, S.V., Halpern, E., and Lackner, A.A. 1998. Simian immunodeficiency virus encephalitis in rhesus macaques is associated with rapid disease progression. *J. Neurovirol.* **4**:260–268.
12. Roberts, E.S., et al. 2004. Acute SIV infection of the brain leads to upregulation of IL6 and interferon-regulated genes: expression patterns throughout disease progression and impact on neuroAIDS. *J. Neuroimmunol.* **157**:81–92.
13. Roberts, E.S., et al. 2006. Host response and dysfunction in the CNS during chronic simian immunodeficiency virus infection. *J. Neurosci.* **26**:4577–4585.
14. Perrella, O., Carrieri, P.B., Guarnaccia, D., and Soscia, M. 1992. Cerebrospinal fluid cytokines in AIDS dementia complex. *J. Neurol.* **239**:387–388.
15. Kolb, S.A., et al. 1999. Identification of a T cell chemotactic factor in the cerebrospinal fluid of HIV-1-infected individuals as interferon-gamma inducible protein 10. *J. Neuroimmunol.* **93**:172–181.
16. Kelder, W., McArthur, J.C., Nance-Sproson, T., McClernon, D., and Griffin, D.E. 1998. Beta-chemokines MCP-1 and RANTES are selectively increased in cerebrospinal fluid of patients with human immunodeficiency virus-associated dementia. *Ann. Neurol.* **44**:831–835.
17. Atlas, A., Gisslen, M., Nordin, C., Lindstrom, L., and Schwieler, L. 2007. Acute psychotic symptoms in HIV-1 infected patients are associated with increased levels of kynurenic acid in cerebrospinal fluid. *Brain Behav. Immun.* **21**:86–91.
18. Coe, C.L., Reyes, T.M., Pauza, C.D., and Reinhard, J.F., Jr. 1997. Quinolinic acid and lymphocyte subsets in the intrathecal compartment as biomarkers of SIV infection and simian AIDS. *AIDS Res. Hum. Retroviruses.* **13**:891–897.
19. Heyes, M.P., et al. 1991. Quinolinic acid in cerebrospinal fluid and serum in HIV-1 infection: relationship to clinical and neurological status. *Ann. Neurol.* **29**:202–209.
20. Gelbard, H.A., et al. 1994. Platelet-activating factor: a candidate human immunodeficiency virus type 1-induced neurotoxin. *J. Virol.* **68**:4628–4635.
21. Heyes, M.P., Lackner, A., Kaufman, S., and Milstien, S. 1991. Cerebrospinal fluid and serum neopterin and biopterin in D-retrovirus-infected rhesus macaques (Macaca mulatta): relationship to clinical and viral status. *AIDS.* **5**:555–560.
22. Want, E.J., Nordstrom, A., Morita, H., and Siuzdak, G. 2007. From exogenous to endogenous: the inevitable imprint of mass spectrometry in metabolomics. *J. Proteome Res.* **6**:459–468.
23. Kawashima, H., et al. 2006. Primary biomarkers in cerebral spinal fluid obtained from patients with influenza-associated encephalopathy analyzed by metabolomics. *Int. J. Neurosci.* **116**:927–936.
24. Smith, C.A., Want, E.J., O'Maille, G., Abagyan, R., and Siuzdak, G. 2006. XCMS: processing mass spectrometry data for metabolite profiling using nonlinear peak alignment, matching, and identification. *Anal. Chem.* **78**:779–787.
25. Smith, C.A., et al. 2005. METLIN: a metabolite mass spectral database. *Ther. Drug Monit.* **27**:747–751.
26. Wishart, D.S., et al. 2007. HMDB: the Human Metabolome Database. *Nucleic Acids Res.* **35**:D521–526.
27. Kanehisa, M., and Goto, S. 2000. KEGG: kyoto encyclopedia of genes and genomes. *Nucleic Acids Res.* **28**:27–30.
28. Bohmer, T., Rydning, A., and Solberg, H.E. 1974. Carnitine levels in human serum in health and disease. *Clin. Chim. Acta.* **57**:55–61.
29. Shihabi, Z.K., Oles, K.S., McCormick, C.P., and Penry, J.K. 1992. Serum and tissue carnitine assay based on dialysis. *Clin. Chem.* **38**:1414–1417.
30. Pilitsis, J.G., et al. 2001. Quantification of free fatty acids in human cerebrospinal fluid. *Neurochem. Res.* **26**:1265–1270.

31. Hoffmann, G.F., et al. 1993. Physiology and pathophysiology of organic acids in cerebrospinal fluid. *J. Inherit. Metab. Dis.* **16**:648–669.
32. Shinawi, M., Gruener, N., and Lerner, A. 1998. CSF levels of carnitine in children with meningitis, neurologic disorders, acute gastroenteritis, and seizure. *Neurology.* **50**:1869–1871.
33. Rubio, J.C., et al. 1998. Cerebrospinal fluid carnitine levels in patients with Alzheimer's disease. *J. Neurol. Sci.* **155**:192–195.
34. Jimenez-Jimenez, F.J., et al. 1997. Cerebrospinal fluid carnitine levels in patients with Parkinson's disease. *J. Neurol. Sci.* **145**:183–185.
35. Pilitsis, J.G., et al. 2003. Free fatty acids in cerebrospinal fluids from patients with traumatic brain injury. *Neurosci. Lett.* **349**:136–138.
36. Pilitsis, J.G., et al. 2003. Measurement of free fatty acids in cerebrospinal fluid from patients with hemorrhagic and ischemic stroke. *Brain Res.* **985**:198–201.
37. Pilitsis, J.G., et al. 2002. Free fatty acids in human cerebrospinal fluid following subarachnoid hemorrhage and their potential role in vasospasm: a preliminary observation. *J. Neurosurg.* **97**:272–279.
38. Neu, I.S. 1983. Essential fatty acids in the serum and cerebrospinal fluid of multiple sclerosis patients. *Acta Neurol. Scand.* **67**:151–163.
39. Mulder, M., et al. 1998. Reduced levels of cholesterol, phospholipids, and fatty acids in cerebrospinal fluid of Alzheimer disease patients are not related to apolipoprotein E4. *Alzheimer Dis. Assoc. Disord.* **12**:198–203.
40. Heyes, M.P., et al. 1992. Relationship of neurologic status in macaques infected with the simian immunodeficiency virus to cerebrospinal fluid quinolinic acid and kynurenic acid. *Brain Res.* **570**:237–250.
41. Heyes, M.P., et al. 1992. Quinolinic acid and kynurenine pathway metabolism in inflammatory and non-inflammatory neurological disease. *Brain.* **115**:1249–1273.
42. Lane, T.E., Buchmeier, M.J., Watry, D.D., and Fox, H.S. 1996. Expression of inflammatory cytokines and inducible nitric oxide synthase in brains of SIV-infected rhesus monkeys: applications to HIV-induced central nervous system disease. *Mol. Med.* **2**:27–37.
43. Giovannoni, G., et al. 1998. Elevated cerebrospinal fluid and serum nitrate and nitrite levels in patients with central nervous system complications of HIV-1 infection: a correlation with blood-brain-barrier dysfunction. *J. Neurol. Sci.* **156**:53–58.
44. Svenningsson, A., Petersson, A.S., Andersen, O., and Hansson, G.K. 1999. Nitric oxide metabolites in CSF of patients with MS are related to clinical disease course. *Neurology.* **53**:1880–1882.
45. Luabeya, M.K., et al. 2000. Blood-brain barrier disruption in simian immunodeficiency virus encephalitis. *Neuropathol. Appl. Neurobiol.* **26**:454–462.
46. Sasseville, V.G., and Lackner, A.A. 1997. Neuropathogenesis of simian immunodeficiency virus infection in macaque monkeys. *J. Neurovirol.* **3**:1–9.
47. Berger, J.R., and Avison, M. 2004. The blood brain barrier in HIV infection. *Front. Biosci.* **9**:2680–2685.
48. Annunziata, P. 2003. Blood-brain barrier changes during invasion of the central nervous system by HIV-1. Old and new insights into the mechanism. *J. Neurol.* **250**:901–906.
49. Marmarou, A. 2003. Pathophysiology of traumatic brain edema: current concepts. *Acta Neurochir. Suppl.* **86**:7–10.
50. Desai, B.S., Monahan, A.J., Carvey, P.M., and Hendey, B. 2007. Blood-brain barrier pathology in Alzheimer's and Parkinson's disease: implications for drug therapy. *Cell Transplant.* **16**:285–299.
51. Williams, K.C., Ulvestad, E., and Hickey, W.F. 1994. Immunology of multiple sclerosis. *Clin. Neurosci.* **2**:229–245.
52. Edmond, J. 2001. Essential polyunsaturated fatty acids and the barrier to the brain: the components of a model for transport. *J. Mol. Neurosci.* **16**:181–193; discussion 215–121.
53. Farooqui, A.A., Horrocks, L.A., and Farooqui, T. 2007. Modulation of inflammation in brain: a matter of fat. *J. Neurochem.* **101**:577–599.
54. Aoki, J., Nagai, Y., Hosono, H., Inoue, K., and Arai, H. 2002. Structure and function of phosphatidylserine-specific phospholipase A1. *Biochim. Biophys. Acta.* **1582**:26–32.
55. Stewart, A., Ghosh, M., Spencer, D.M., and Leslie, C.C. 2002. Enzymatic properties of human cytosolic phospholipase A(2)gamma. *J. Biol. Chem.* **277**:29526–29536.
56. Haughey, N.J., et al. 2004. Perturbation of sphingolipid metabolism and ceramide production in HIV-dementia. *Ann. Neurol.* **55**:257–267.
57. Briscoe, C.P., et al. 2003. The orphan G protein-coupled receptor GPR40 is activated by medium and long chain fatty acids. *J. Biol. Chem.* **278**:11303–11311.
58. Keller, H., et al. 1993. Fatty acids and retinoids control lipid metabolism through activation of peroxisome proliferator-activated receptor-retinoid × receptor heterodimers. *Proc. Natl. Acad. Sci. U. S. A.* **90**:2160–2164.
59. Meyer zu Heringdorf, D., and Jakobs, K.H. 2007. Lysophospholipid receptors: signalling, pharmacology and regulation by lysophospholipid metabolism. *Biochim. Biophys. Acta.* **1768**:923–940.
60. Bellizzi, M.J., Lu, S.M., Masliah, E., and Gelbard, H.A. 2005. Synaptic activity becomes excitotoxic in neurons exposed to elevated levels of platelet-activating factor. *J. Clin. Invest.* **115**:3185–3192.
61. Stock, C., Schilling, T., Schwab, A., and Eder, C. 2006. Lysophosphatidylcholine stimulates IL-1beta release from microglia via a P2X7 receptor-independent mechanism. *J. Immunol.* **177**:8560–8568.
62. Burdo, T.H., Marcondes, M.C., Lanigan, C.M., Penedo, M.C., and Fox, H.S. 2005. Susceptibility of Chinese rhesus monkeys to SIV infection. *AIDS.* **19**:1704–1706.
63. Lane, T.E., Buchmeier, M.J., Watry, D.D., Jakubowski, D.B., and Fox, H.S. 1995. Serial passage of microglial SIV results in selection of homogeneous env quasispecies in the brain. *Virology.* **212**:458–465.
64. Horn, T.F.W., et al. 1998. Early physiological abnormalities after simian immunodeficiency virus infection. *Proc. Natl. Acad. Sci. U. S. A.* **95**:15072–15077.
65. Roberts, E.S., et al. 2003. Induction of pathogenic sets of genes in macrophages and neurons in neuroAIDS. *Am. J. Pathol.* **162**:2041–2057.